PHOTONICS Research

Numerical investigations of an optical switch based on a silicon stripe waveguide embedded with vanadium dioxide layers

Lei Chen, Han Ye, Yumin Liu,* Dong Wu, Rui Ma, and Zhongyuan Yu

State Key Laboratory of Information Photonics and Optical Communications, Beijing University of Posts and Telecommunications, Beijing 100876, China
**Corresponding author: microliuyumin@hotmail.com*

Received 6 March 2017; revised 11 April 2017; accepted 4 May 2017; posted 4 May 2017 (Doc. ID 288086); published 10 July 2017

A novel scheme for the design of an ultra-compact and high-performance optical switch is proposed and investigated numerically. Based on a standard silicon (Si) photonic stripe waveguide, a section of hyperbolic metamaterials (HMM) consisting of 20-pair alternating vanadium dioxide (VO_2)/Si thin layers is inserted to realize the switching of fundamental TE mode propagation. Finite-element-method simulation results show that, with the help of an HMM with a size of 400 nm × 220 nm × 200 nm (width × height × length), the ON/OFF switching for fundamental TE mode propagation in an Si waveguide can be characterized by modulation depth (MD) of 5.6 dB and insertion loss (IL) of 1.25 dB. It also allows for a relatively wide operating bandwidth of 215 nm maintaining MD > 5 dB and IL < 1.25 dB. Furthermore, we discuss that the tungsten-doped VO_2 layers could be useful for reducing metal-insulator-transition temperature and thus improving switching performance. In general, our findings may provide some useful ideas for optical switch design and application in an on-chip all-optical communication system with a demanding integration level.

OCIS codes: (130.4815) Optical switching devices; (230.3120) Integrated optics devices; (160.3918) Metamaterials.

https://doi.org/10.1364/PRJ.5.000335

1. INTRODUCTION

Recent years have seen promising development of photonic devices that are based on a great variety of functional micro-/nano-structures and conventional or alternative plasmonic materials, which include optical interconnects, modulators, detectors, splitters, switches, mode converters, lasers, and so on [1–7]. Among them, it is still a challenge for the full implementation of all-optical switches because they are always expected to feature milliwatt power consumption, picosecond switching time, and tenth-decibel insertion loss (IL). In addition, we also characterize all-optical switches with high compactness and large modulation depth (MD) in an on-chip optical communication system [8]. Researchers have performed numerous numerical and experimental work on switch design utilizing the resonance cavity effect [5], optical interference [9], phase-change property [10], light saturation absorption [11,12], and so on. As we all know, in the near-infrared region, conventional metals (e.g., gold, silver, copper, and aluminum) are extensively used in photonic devices due to their good plasmonic behavior and low optical loss, despite the fact that they have low melting temperature, relative softness, and metal contamination to surrounding mediums in the form of ion diffusion [13]. Nevertheless, the promising alternative plasmonic materials have greatly surprised us because of the tunable optical property, CMOS-compatibility, chemical stability, and high-temperature durability [14]. They could be, for example, transition metal nitrides (e.g., titanium nitride, zirconium nitride, hafnium nitride), transparent conducting oxides (e.g., indium-tin-oxide, aluminum-doped zinc oxide, germanium-doped zinc oxide), phase-change materials [e.g., vanadium dioxide (VO_2)], 2D materials (e.g., graphene, hexagonal boron nitride), or high-doping semiconductors (e.g., silicon, germanium) [14–18]. Furthermore, these plasmonic materials are widely used in combination with specific dielectrics. Specifically, we can use gold/silver combined with alumina in ultraviolent regions, gold/silver combined with titanium oxides in visible regions, titanium nitride/indium tin oxides combined with silicon or silicon dioxide in near-infrared regions, and indium-gallium-arsenide/graphene combined with alumina in mid-infrared even terahertz regions [19].

The material of VO_2 is essential for applications in all-optical computing, optical communication, and smart laser shielding for military use. Among a series of vanadium oxides with variable valence (e.g., V_2O_3, V_2O_5), the distinct feature of VO_2 is the reversible metal-to-insulator transition (MIT) behavior at a critical temperature of about $T_{MIT} = 340$ K (68°C), which brings in sharp optical contrast from high transmittance to reflectance with

greatly varied permittivity for a near-infrared light wave [20]. This is because, with room temperature approaching to T_{MIT}, the lattice structure of a VO_2 film will change from monoclinic insulating phase to a tetragonal metallic phase, which causes its electrical conductivity increased by several orders of magnitudes. The optical property of VO_2 film can be tuned thermally, electrically, magnetically, and by strain [21]. Furthermore, we could probably promote electrical and optical properties of VO_2 by manipulating its T_{MIT}. The tunability significantly facilitates the development of room-temperature infrared detection and optical switching.

In this paper, to remove complex and bulky structures, we propose that the silicon photonic (Si) waveguide inserted with a section of hyperbolic material (HMM) can be exploited as an optical switch. On the one hand, HMM is an artificial structure with manageable electromagnetic properties that cannot be obtained from conventional structures. Merely the most basic structure consisting of alternating metal/insulator layers can induce a strong absorption effect or become transparent to an incoming light wave [22]. On the other hand, the HMM structure greatly contributes to complete light–matter interaction. Therefore, propagation of the dominant TE mode in the Si stripe waveguide can be controlled by a well-designed HMM. The designed structure can achieve ON/OFF switching functionality after laser irradiation [23]. Alternatively, the VO_2 layers also can be extended to contact with metal electrodes for active electric control. To the best of our knowledge, the proposed optical switch has been neither studied nor previously reported.

2. NUMERICAL SIMULATION

A. Design and Modeling

Figure 1 shows a schematic view of the proposed optical switch without keeping the geometry ratio. With embedded VO_2 layers, the Si stripe waveguide (WG) has a standard cross-section of $W \times H = 400$ nm × 220 nm, with length of $L_{in} + L_{HMM} + L_{out}$. It can be divided into three parts: input WG_1 with $L_{in} = 1$ μm, HMM structure with $L_{HMM} = (d_m + d_d) \times N$, and output WG_2 with $L_{out} = 1$ μm. The parameters of d_m, d_d, and N indicate the length of a VO_2 layer, length of a Si layer, and number of VO_2/Si pairs, respectively. Considering device compactness, we vary the values of d_m and d_d from 5 to 55 nm, and set $N = 20$. Performed in the wave-optics module of COMSOL Multiphysics software, finite-element-method boundary mode analysis combined with perfectly matched layers is used to solve the 2D model, as shown in Fig. 1(b). Numerical port is set to launch the dominant fundamental TE mode. For the accuracy and convergence of simulation results, we discretize the device structure using high-quality mapping mesh and boundary layer.

The refractive indices of Si, SiO_2, and air are set as 3.48, 1.45, and 1, respectively [24]. Here we use experimental refractive index $(\tilde{n} = n + ik)$ of $\tilde{n}_{exp}(M) = 2.1313 + 2.844i$ for the metallic VO_2 after MIT process and $\tilde{n}_{exp}(D) = 3.1309 + 0.3612i$ for dielectric VO_2 in normal state [25]. Based on the effective medium method [26,27], we can consider the 20-pair VO_2/Si layers as a section of HMM, with optical property characterized by the effective tensor parallel $\{\varepsilon_x = 1/[\rho/\varepsilon_m + (1-\rho)/\varepsilon_d]\}$ and perpendicular $[\varepsilon_y = \rho\varepsilon_m + (1-\rho)\varepsilon_d]$ to the anisotropy axis (x axis in our model). The metal filling factor of $\rho = d_m/(d_m + d_d)$ is set as 0.5 for ease of control. Note that for a material, the real part n indicates impedance matching, while the imaginary part k indicates absorption ability.

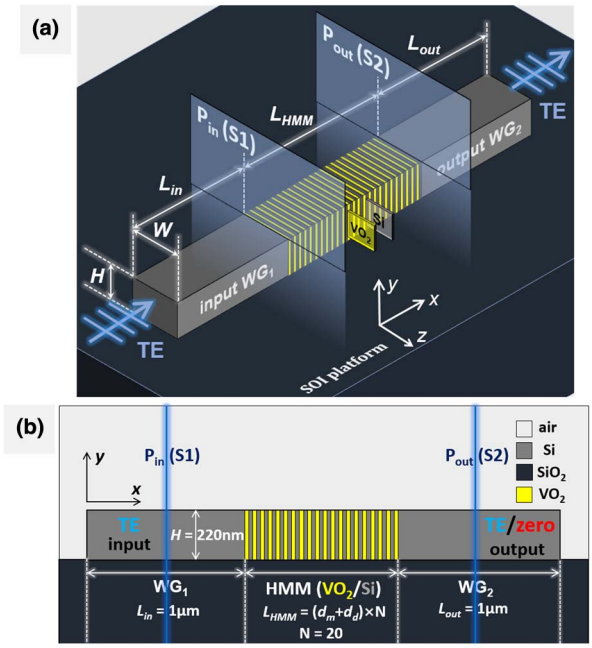

Fig. 1. (a) 3D and (b) lateral view of the proposed optical switch inserted with an HMM structure consisting of 20-pair alternating VO_2/Si layers on a glass substrate.

Next, we use three performance indices to evaluate the optical switch [2,5]. We first denote the x component of power flux density as *Poavx*. Then the optical power input/output the optical switch is calculated as the integral value of *Poavx* along boundary S1/S2, which is labeled as P_{in}/P_{out} in Fig. 1(b). Accordingly, the TE mode transmittance is defined as $T_{ON}(D) = P^D_{out}/P^D_{in}$ for "ON" state and $T_{OFF}(M) = P^M_{out}/P^M_{in}$ for "OFF" state. Therefore, performance indices of MD and IL can be calculated by expressions of MD $= (T_{ON} - T_{OFF})/T_{ON}$ (dimensionless)/MD (dB) $= 10\log_{10}(T_{ON}/T_{OFF})$ and IL(dB) $= -10\log_{10}(T_{ON})$, respectively [5]. We also calculate the operating bandwidth (BW) that is a wavelength range maintaining MD > 5 dB. An optical switch with MD higher than 5 dB is sufficient and practicable as validated in Ref. [10].

B. Results and Discussion

We first explore how absorption losses caused by k of $\tilde{n}_{exp}(M)$ and $\tilde{n}_{exp}(D)$ control the switching performance. In Fig. 2(a), for k of $\tilde{n}_{exp}(D)$ varying from 0.0 to 0.5, all $T_{ON}(D)$ rapidly decrease as VO_2 layer length d_m increases. Note that nearly perfect transmission efficiency can be obtained when $k = 0$ due to good impedance matching and zero absorption loss. Furthermore, shorter HMM can cause fewer losses to the TE mode. In Fig. 2(b), the curve of MD shows a different tendency with that of $T_{ON}(D)$ due to the great impact of $\tilde{n}_{exp}(M)$ on $T_{OFF}(M)$. As a result, we can design a high-performance optical switch by following the MD index (note that the IL is not considered here).

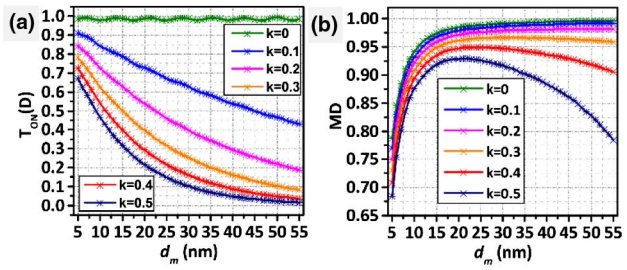

Fig. 2. (a) Transmittance diagram of T_{ON} based on dielectric VO_2 layers with varying k of $\tilde{n}_{\mathrm{exp}}(D)$. (b) Using the same dielectric VO_2 layers with constant $\tilde{n}_{\mathrm{exp}}(D) = 3.1309 + 0.3612i$, relationship curve of MD-d_m is calculated based on metallic VO_2 layers for different k of $\tilde{n}_{\mathrm{exp}}(M)$.

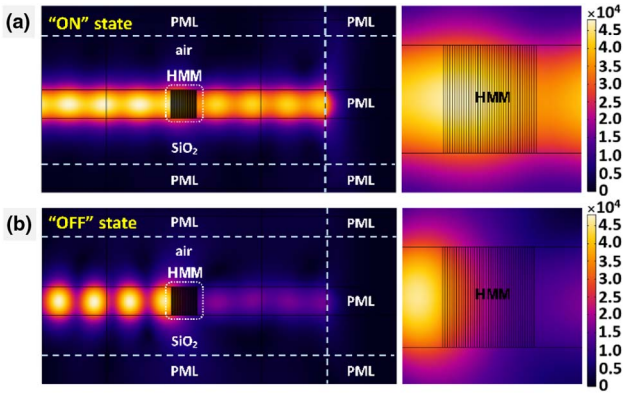

Fig. 3. Electric field distribution of TE mode propagation for (a) "ON" and (b) "OFF" state with zoom-in views of the HMM structure.

Then we make an intuitive presentation of the "ON"/"OFF" switching by plotting the norm electric field distribution, as shown in Fig. 3. We base the following simulation on an ultra-compact HMM with $d_m = 5$ nm ($L_{\mathrm{HMM}} = 200$ nm). It can be clearly seen that, for the "ON" state, the TE mode can pass through WG_2 with an undistorted field profile and slightly weakened field intensity. However, for the "OFF" state, the field intensity of TE mode is rapidly reduced. Furthermore, as shown in Fig. 4, we plot the *Poavx* distribution and total

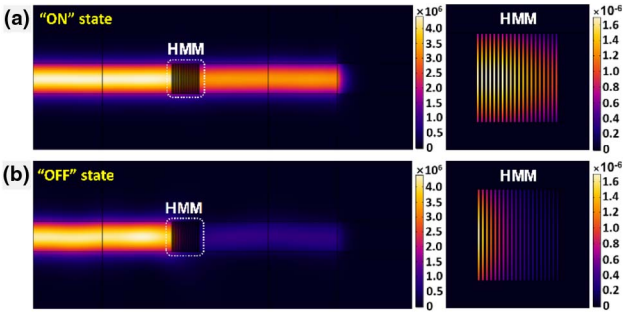

Fig. 4. Power flux density *Poavx* distribution of TE mode propagation for (a) "ON" and (b) "OFF" state with zoom-in views of the HMM structure.

electromagnetic losses caused by HMM. Figure 4(a) shows the normal propagation without radiation. In the "OFF" state, it is indicated that the TE mode is effectively isolated by the HMM with little radiation power. This means a lot to the integration with other components because it could cause little crossing disturbance.

Next, we explore the propagation loss mechanism of the HMM inserted Si waveguide. The losses of the TE mode can be caused by HMM-induced absorption, reflection, and radiation. Figure 5 illustrates that HMM will cause zero/little reflection to the TE mode when it operates in the "ON"/"OFF" state. Two points are worth mentioning: first, seeing that the effect of k on $T_{\mathrm{ON}}(D)$ has been simulated in Fig. 2(a), here we use $\tilde{n}_{\mathrm{exp}}(D) = 3.1309$ in Fig. 5(a), which is helpful in explaining the impedance matching. Regardless of the difference of refractive index between Si (3.48) and dielectric VO_2 (3.1309), the switch can still perform well with a 2.2 μm long HMM. Second, the reflection curve obtained from Fig. 5(b) well explains the standing pattern in WG_1 from Fig. 3(b). Furthermore, Fig. 6 gives an intuitive view of the electric field intensity distribution, which indicates that the power radiated into surrounding mediums is negligible. We therefore conclude that the propagation loss is mainly resulted from absorption. It can be explained by the effective relative permittivity of HMM. Calculation results show that the HMM structure will present an anisotropic optical property with $\varepsilon_x = 4.2823 + 6.06i$ and $\varepsilon_y = 12.818 + 16.14i$ ($n_y = 2.4191 + 1.253i$) when VO_2 behaves as a metal. As a result, for one thing, the noticed reflection in Fig. 5(b) is due to the reduced refractive index from 3.48 to 2.4191 at the WG_1/HMM interface. For another

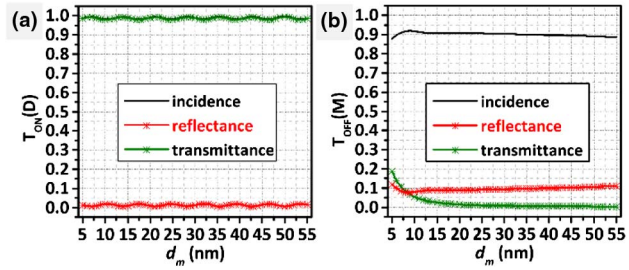

Fig. 5. Transmission diagram of (a) $T_{\mathrm{ON}}(D)$ and (b) $T_{\mathrm{OFF}}(M)$ for an optical switch with d_m varying from 5 to 55 nm.

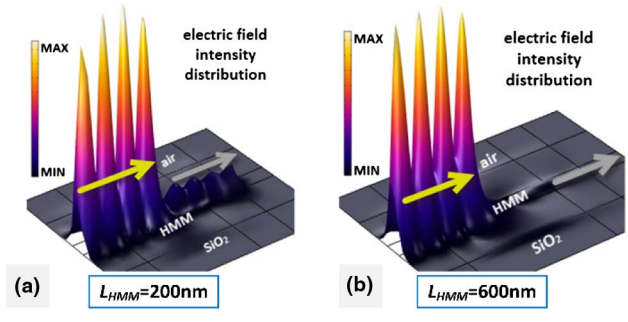

Fig. 6. Electric field intensity distribution in an optical switch in"OFF" state with different HMM length of (a) $L_{\mathrm{HMM}} = 200$ nm ($d_m = d_d = 5$ nm) and (b) $L_{\mathrm{HMM}} = 600$ nm ($d_m = d_d = 15$ nm).

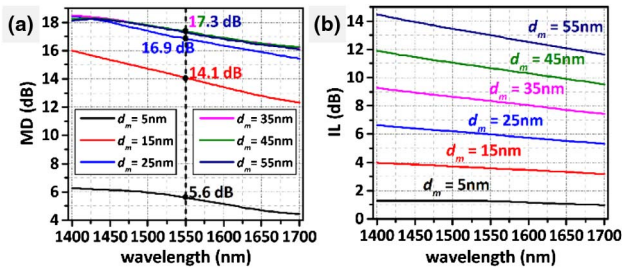

Fig. 7. Calculated (a) MD and (b) IL as a function of wavelength with d_m (L_{HMM}) varying from 5 nm (200 nm) to 55 nm (2200 nm).

thing, the significantly increased k values of 6.06 and 16.14 are responsible for the huge absorption of the TE mode. In other words, compared with pure metal or insulator, the HMM structure consisting of alternating metal/insulator layers shows desirable optical property very dissimilar to that of either metal or insulator.

Last, as shown in Fig. 7, we discuss the propagation loss introduced by HMM length and calculate the device operating BW. On one hand, Fig. 7 indicates that the length of HMM structure plays a decisive role in device performance. That is, a too-long HMM structure will cause huge loss to the TE mode when the device operates either in the "ON" or "OFF" state. On the other hand, the device can achieve a wide operating BW of 215 nm with MD > 5 dB while maintaining a constant IL of 1.25 dB. Therefore, considering the balance between MD and IL, an optical switch characterized by an ultra-compact footprint of 400 nm × 220 nm × 200 nm (width × height × length), moderate MD of 5.6 dB, and IL of 1.25 dB is our first choice.

3. SWITCHING FEATURE OF DOPED VO_2

Based on the experiments reported in Refs. [28,29], we know that an undoped VO_2 film has MIT temperature of T_{MIT} = 68°C and temperature window of merely 1°C–2°C. However, the T_{MIT} could be manipulated by chemical doping. For example, we could reduce T_{MIT} utilizing doping elements of W, Mo, Nb, Ta, F, Te, Fe, etc., increase T_{MIT} utilizing doping elements of Al, Ge, Ga, etc., and simply change T_{MIT} utilizing doping elements of Cu and Ti. Making continuous optical modulation a reality, tungsten (W)-doped VO_2 thin film works best. This is because it achieves not only a reduced T_{MIT}, but also a relatively wide temperature window. We can also expect to obtain the following advantages. First, the switching time could be largely improved because of the doping percent influenced electrical conductivity. Second, the W-doped VO_2 could get its absorbing ability promoted during MIT process. Third, the reduced T_{MIT} could protect the Si waveguide and other components from laser damage, because the time of MIT process is greatly shortend. In general, a relatively low T_{MIT} is beneficial for optical switching performance. To simulate the effect of doping-induced complex refractive index variation on device performance, MD is calculated as a function of real part n and imaginary part k of $\tilde{n}_{exp}(M)$. It is worth noting that there is no accurate relationship between complex refractive index and chemical doping percent so far. Therefore, Fig. 8 indicates a possibility of improving the switching performance.

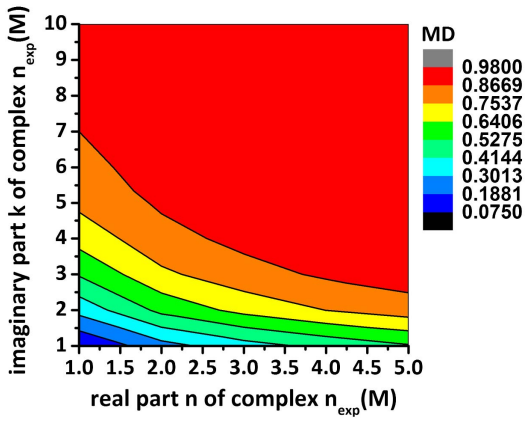

Fig. 8. Based on an optical switch using W-doped VO_2 layers (d_m = 5 nm), MD varies as a function of both n and k of $\tilde{n}_{exp}(M)$.

4. EXPERIMENTAL FEASIBILITY

With support from some reported experimental work [28–30], we discuss the practicable experimental processes despite the fact that our design is based on numerical simulations. First, on the silicon-on-insulator (SOI) platform, the WG and Si layers in HMM can be written using electron beam lithography (EBL). Second, VO_2 layers in HMM can be directly prepared on Si waveguide using pulsed laser deposition. Finally, shaping the device with required dimension can be realized using EBL again. In addition, the element of W can be doped in VO_2 film co-sputtering a W wire during the film deposition process [28].

5. CONCLUSION

In summary, we numerically demonstrate an ultra-compact silicon waveguide-based optical switch utilizing a multilayer hyperbolic metamaterial. Under laser irradiation, the Si waveguide inserted with an HMM with size of 400 nm × 220 nm × 200 nm (width × height × length) could offer good ON/OFF switching performance with MD of 5.6 dB, low IL of 1.25 dB, and operating BW of 215 nm. Furthermore, the SOI-based simple and compact device structure makes it easy to cooperate with other components in an on-chip integrated circuit. We also can dope the VO_2 layer with a variety of elements to realize continuous modulation of its optical property. In general, our findings may provide some useful ideas for optical switch design and application in an on-chip all-optical communication system with demanding integration level.

Funding. Ministry of Science and Technology of the People's Republic of China (MOST) (2016YFA0301300); National Natural Science Foundation of China (NSFC) (61275201, 61372037); Beijing University of Posts and Telecommunications (BUPT) Excellent Ph.D. Students Foundation (CX2016204); Fundamental Research Funds for the Central Universities (2016RC24); Beijing Excellent Ph.D. Thesis Guidance Foundation (20131001301).

REFERENCES

1. C. Wan, T. K. Gaylord, and M. S. Bakir, "Grating design for interlayer optical interconnection of in-plane waveguides," Appl. Opt. **55**, 2601–2610 (2016).
2. G. T. Reed, G. Mashanovich, F. Y. Gardes, and D. J. Thomson, "Silicon optical modulators," Nat. Photonics **4**, 518–526 (2010).
3. J. Wang, Z. Cheng, Z. Chen, X. Wan, B. Zhu, H. K. Tsang, C. Shu, and J. Xu, "High-responsivity graphene-on-silicon slot waveguide photodetectors," Nanoscale **8**, 13206–13211 (2016).
4. K. Wen, Y. Hu, L. Chen, J. Zhou, L. Lei, and Z. Guo, "Design of an optical power and wavelength splitter based on subwavelength waveguides," J. Lightwave Technol. **32**, 3020–3026 (2014).
5. P. Dastmalchi and G. Veronis, "Plasmonic switches based on subwavelength cavity resonators," J. Opt. Soc. Am. B **33**, 2486–2492 (2016).
6. J. Kim, S. Y. Lee, H. Park, K. Lee, and B. Lee, "Reflectionless compact plasmonic waveguide mode converter by using a mode-selective cavity," Opt. Express **23**, 9004–9013 (2015).
7. Y. Li and W. P. Huang, "Electrically-pumped plasmonic lasers based on low-loss hybrid SPP waveguide," Opt. Express **23**, 24843–24849 (2015).
8. A. Emboras, C. Hoessbacher, C. Haffner, W. Heni, U. Koch, P. Ma, Y. Fedoryshyn, J. Niegemann, C. Hafner, and J. Leuthold, "Electrically controlled plasmonic switches and modulators," IEEE J. Sel. Top. Quantum Electron. **21**, 276–283 (2015).
9. P. P. Sahu, "Theoretical investigation of all optical switch based on compact surface plasmonic two mode interference coupler," J. Lightwave Technol. **34**, 1300–1305 (2016).
10. B. Gholipour, J. Zhang, K. F. MacDonald, D. W. Hewak, and N. I. Zheludev, "An all-optical, non-volatile, bidirectional, phase-change meta-switch," Adv. Mater. **25**, 3050–3054 (2013).
11. J. Li, J. Tao, Z. H. Chen, and X. G. Huang, "All-optical controlling based on nonlinear graphene plasmonic waveguides," Opt. Express **24**, 22169–22176 (2016).
12. G. X. Ni, L. Wang, M. D. Goldflam, M. Wagner, Z. Fei, A. S. McLeod, M. K. Liu, F. Keilmann, B. Özyilmaz, A. H. C. Neto, J. Hone, M. M. Fogler, and D. N. Basov, "Ultrafast optical switching of infrared plasmon polaritons in high-mobility graphene," Nat. Photonics **10**, 244–247 (2016).
13. G. V. Naik, V. M. Shalaev, and A. Boltasseva, "Alternative plasmonic materials: beyond gold and silver," Adv. Mater. **25**, 3264–3294 (2013).
14. G. V. Naik, J. Kim, and A. Boltasseva, "Oxides and nitrides as alternative plasmonic materials in the optical range," Opt. Express **1**, 1090–1099 (2011).
15. A. Lalisse, G. Tessier, J. Plain, and G. Baffou, "Plasmonic efficiencies of nanoparticles made of metal nitrides (TiN, ZrN) compared with gold," Sci. Rep. **6**, 38647 (2016).
16. V. E. Babicheva, A. Boltasseva, and A. V. Lavrinenko, "Transparent conducting oxides for electro-optical plasmonic modulators," Nanophotonics **4**, 165–185 (2015).
17. C. T. Riley, J. S. T. Smalley, K. W. Post, D. N. Basov, Y. Fainman, D. Wang, Z. Liu, and D. J. Sirbuly, "High-quality, ultraconformal aluminum-doped zinc oxide nanoplasmonic and hyperbolic metamaterials," Small **12**, 892–901 (2016).
18. R. Alaee, M. Albooyeh, S. Tretyakov, and C. Rockstuhl, "Phase-change material-based nanoantennas with tunable radiation patterns," Opt. Lett. **41**, 4099–4102 (2016).
19. P. Shekhar, J. Atkinson, and Z. Jacob, "Hyperbolic metamaterials: fundamentals and applications," Nano Convergence **1**, 14 (2014).
20. J. H. Choe and J. T. Kim, "Design of vanadium oxide-based plasmonic modulator for both TE and TM modes," IEEE Photon. Technol. Lett. **27**, 514–517 (2015).
21. S. B. Choi, J. S. Kyoung, H. S. Kim, H. R. Park, B. J. Kim, Y. H. Ahn, F. Rotermund, H. T. Kim, K. J. Ahn, and D. S. Kim, "Nanopattern enabled terahertz all-optical switching on vanadium dioxide thin film," Appl. Phys. Lett. **98**, 071105 (2011).
22. A. Poddubny, I. Iorsh, P. Belov, and Y. Kivshar, "Hyperbolic metamaterials," Nat. Photonics **7**, 948–957 (2013).
23. D. W. Ferrara, E. R. MacQuarrie, V. D. B. J. Nag, A. B. Kaye, and R. F. H. Jr, "Plasmonic enhancement of the vanadium dioxide phase transition induced by low-power laser irradiation," Appl. Phys. A **108**, 255–261 (2012).
24. L. Chen, Y. Liu, Z. Yu, D. Wu, R. Ma, Y. Zhang, and H. Ye, "Numerical investigations of a near-infrared plasmonic refractive index sensor with extremely high figure of merit and low loss based on the hybrid plasmonic waveguide-nanocavity system," Opt. Express **24**, 23260–23270 (2016).
25. M. Kim, J. Jeong, J. K. S. Poon, and G. V. Eleftheriades, "Vanadium-dioxide-assisted digital optical metasurfaces for dynamic wavefront engineering," J. Opt. Soc. Am. B **33**, 980–988 (2016).
26. T. Li and J. B. Khurgin, "Hyperbolic metamaterials: beyond the effective medium theory," Optica **3**, 1388–1396 (2016).
27. V. E. Babicheva, M. Y. Shalaginov, S. Ishii, A. Boltasseva, and A. V. Kildishev, "Finite-width plasmonic waveguides with hyperbolic multilayer cladding," Opt. Express **23**, 9681 (2015).
28. G. K. Bebek, M. N. F. Hoqie, M. Holtz, Z. Fan, and A. A. Bernussi, "Continuous tuning of W-doped VO_2 optical properties for terahertz analog applications," Appl. Phys. Lett. **105**, 201902 (2014).
29. T. Wang, H. Yu, X. Dong, Y. D. Jiang, and R. L. Hu, "Modeling and experiments of N-doped vanadium oxide prepared by a reactive sputtering process," Chin. Phys. B **24**, 038102 (2015).
30. R. M. Briggs, I. M. Pryce, and H. A. Atwater, "Compact silicon photonic waveguide modulator based on the vanadium dioxide metal-insulator phase transition," Opt. Express **18**, 11192–11201 (2010).